Journal of Structural Geology 32 (2010) 727–740

Contents lists available at ScienceDirect

Journal of Structural Geology

journal homepage: www.elsevier.com/locate/jsg

Structural analysis of fault populations along the oblique, ultra-slow spreading Knipovich Ridge, North Atlantic Ocean, 74°30′N-77°50′N

Daniel Curewitz [a,*], Kyoko Okino [b], Miho Asada [b], Boris Baranov [c], Evgeny Gusev [d], Kensaku Tamaki [b,e]

[a] Syracuse University, Department of Earth Sciences, 204 Heroy Geology Laboratory, Syracuse, NY 13244, USA
[b] Ocean Research Institute, University of Tokyo, 1-15-1 Minamidai, Nakano, Tokyo 164-8639, Japan
[c] Shirshov Institute of Oceanology RAS, 36 Hakhimovsky, Moscow 117851, Russia
[d] VNIIOkeangeologia, 1 Anglyiiski Av., St. Petersburg 190121, Russia
[e] University of Tokyo, School of Engineering, 3-1 Hongo, Bunkyo-ku, Tokyo 113-8656, Japan

ARTICLE INFO

Article history:
Received 7 November 2008
Received in revised form
9 July 2009
Accepted 7 August 2009
Available online 18 August 2009

Keywords:
Fault populations
Oblique rifting
Segmentation
Mid-Ocean Ridge

ABSTRACT

The Knipovich Ridge (73°30′–78°40′N) is an extreme end-member of the mid-ocean ridge spreading system, both in terms of spreading rate (<1.5 cm/yr) and angle between the ridge and the spreading direction (40°–53°). Structural analysis of side-scan sonar images obtained along ~400 km of the ridge axis reveals systematic relationships between fault population parameters, obliquity, and axial segmentation along the ridge.

Fault population characteristics conform to observational and experimental analyses of oblique rifting and spreading systems. For the ridge as a whole, faults in the axial region are short, straight, isolated (not linked into complex fault zones), and exhibit length-scaling relationships characteristic of young and active fault systems. Faults are generally oblique to both the ridge axis and the spreading direction, and orientations vary systematically with angle between ridge and spreading direction.

Along-axis analysis reveals the influence of axial segmentation on fault population characteristics. Segment centers are dominated by faults perpendicular and sub-perpendicular to plate motion with longer characteristic length and generally lower fracture density. Conversely, segment ends are dominated by faults striking oblique to plate motion with shorter characteristic length and generally higher fracture density. We infer that faulting in segment centers is strongly influenced by the mechanical effects of dike intrusion perpendicular to plate motion, while faulting in segment ends is controlled by the mechanics of oblique rifting, non-transform discontinuities, and/or accommodation zones. The contrasts between these distinct structural and mechanical settings along the ridge axis are accentuated by the high obliquity and ultra-slow spreading rate of this spreading system.

1. Introduction

1.1. Study area

The Knipovich Ridge lies in the northern Norwegian-Greenland Sea, Northeast Atlantic, just off the coast of the Eurasian continental margin (Fig. 1a). It is situated asymmetrically between Svalbard and NE Greenland, and extends from 73°30′N to 78°40′N, from the junction with the Mohns Ridge to the Molloy Transform. It is one of the slowest and most obliquely spreading mid-ocean ridges on the planet. The ridge trends ~347° from 74°30′ to 75°50′N, and ~000° from 75°50′N to 78°40′N. The NUVEL-1A and REVEL (DeMets et al., 1990, 1994; Sella et al., 2002) global circuit plate-tectonic models predict a plate motion vector of ~307° and a full spreading rate of ~1.4 cm/yr (Fig. 1b). The ridge axis is highly oblique to the spreading direction, with an angle between the spreading vector and the ridge axis (noted as "alpha" after Withjack and Jamison, 1986) ranging from 37° in the north to 50° in the south.

Magnetic anomaly data are sparse, and interpretations vary drastically (e.g. Crane et al., 1991; Vogt et al., 1998; Skogseid et al., 2000), however Vogt et al. (1998) provide a tentative identification of magnetic anomaly lineations in the Northeast Atlantic based on compiled ship and aeromagnetic surveys (Olesen et al., 1997). These interpretations reveal discrete packages of short, discontinuous anomalies that trend oblique to the ridge axis and nearly perpendicular to the relative plate motion vector. These packages are bounded by approximately linear, plate-motion-

* Corresponding author. Tel.: +1 315 530 5481; fax: +1 315 443 3363.
E-mail address: dcurewit@syr.edu (D. Curewitz).

0191-8141/$ – see front matter © 2009 Elsevier Ltd. All rights reserved.
doi:10.1016/j.jsg.2009.08.011

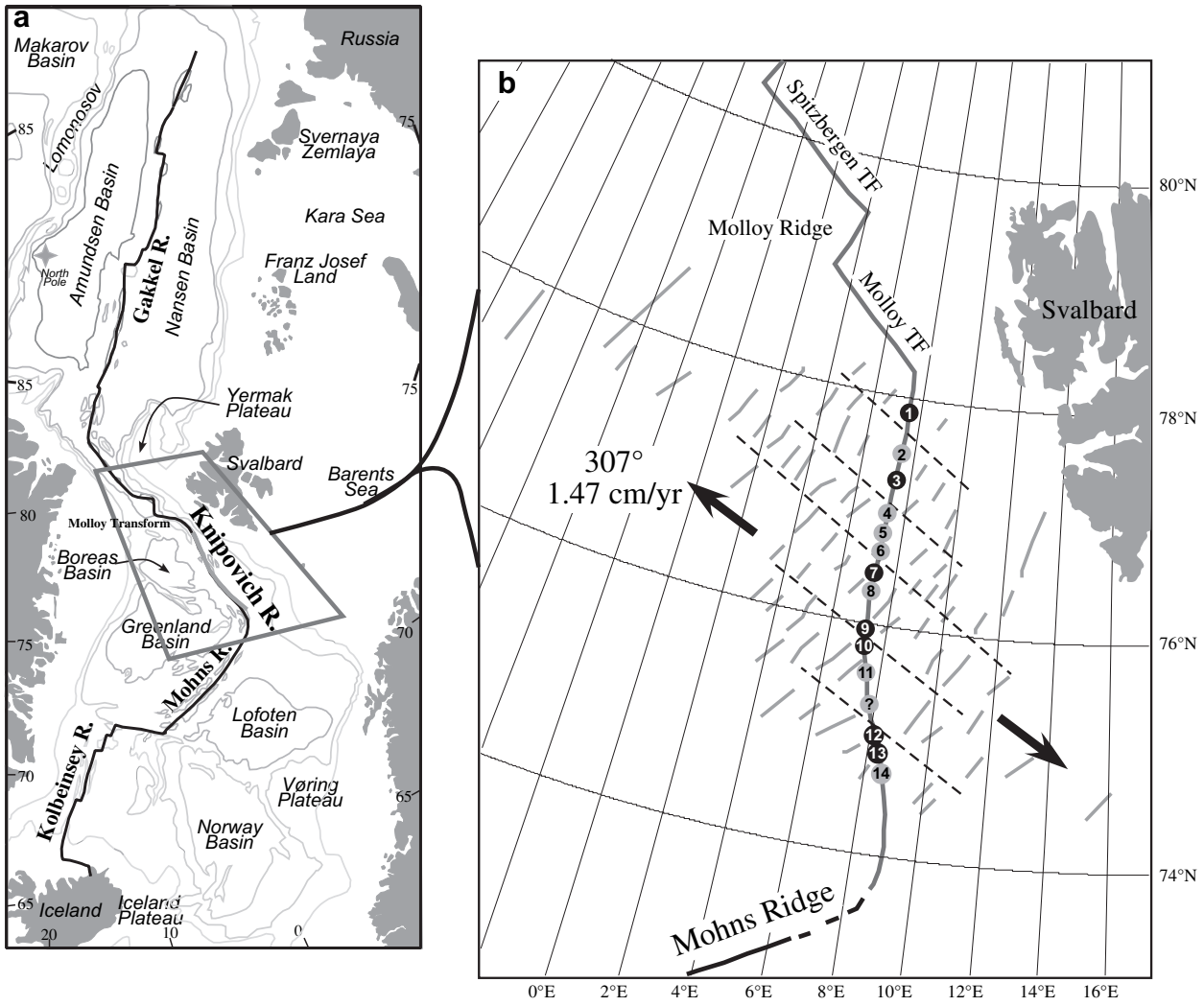

Fig. 1. a) Polar stereographic projection showing the location of Arctic mid-ocean ridges, continental land masses, and 1000 m contours of ocean basin depths. The location of the September, 2000 survey is shown by the bold gray line. b) Stereographic projection showing Svalbard, the Knipovich Ridge, tentative magnetic anomaly lineations and non-transform discontinuities (after Olesen et al., 1997; Vogt et al., 1998). The numbered circles correspond to spreading segment centers identified by Okino et al. (2002). Black circles correspond to segment centers that lie at the intersection of off-axis seamount chains with the ridge, and have more pronounced relief, sonar reflectance, and mantle Bouguer anomalies. Gray circles correspond to weaker spreading segments. One gray circle (with "?") corresponds to an area with an identified mantle Bouguer anomaly that has no obvious bathymetric or reflectance signature. The plate motion vector is taken from DeMets et al. (1990, 1994) and Sella et al. (2002).

parallel regions of low magnetization and are interpreted as possible traces of spreading discontinuities (Fig. 1b, after Vogt et al., 1998).

Previous work on the Knipovich Ridge (Crane et al., 1991, 2001; Crane and Solheim, 1995; Vogt et al., 1998; Gusev and Shkarubo, 2001; Okino et al., 2002) has delineated a 3000–3500 m deep, 10–15 km wide rift valley punctuated by widely spaced (20–40 km), en echelon volcanic highs ranging from 0.5 to 1 km in height above the seafloor (Fig. 2a, 2b). The axial seamounts commonly lie along the trend of chains of off-axis highs (Fig. 2b), suggesting that they represent relatively stable loci of magmatic accretion (Okino et al., 2002). The most prominent axial volcanic highs are located at the intersection of the discrete packages of magnetic anomalies and the ridge axis (shaded circles in Fig. 1b).

Sediment thickness on the axial valley floor (up to 100 m) and flanks (up to 1 km or more) is high owing to the proximity of the Eurasian continental shelf (Vogt and Sundvor, 1996; Vogt et al., 1998; Sundvor et al., 2000; Gusev and Shkarubo, 2001). Seismic activity is generally low, and earthquakes are widely scattered in the rift valley and on the eastern (Eurasian) flank of the ridge (Crane et al., 1991; Gusev and Shkarubo, 2001).

1.2. Knipovich Ridge morphology and segmentation

Mid-ocean ridge segmentation is defined in terms of axial depth profiles and the mantle Bouguer anomaly (MBA) profile. MBA profiles are used to investigate density variations in the mantle in order to determine the pattern of mantle upwelling and melt distribution beneath a spreading segment. High and low MBA values are interpreted to represent denser/colder mantle with lower magma production potential, or lighter/warmer mantle with higher magma production potential, respectively. Ridge axis discontinuities generally occur at local depth maxima and correspond to high MBA values (Kuo and Forsyth, 1988; Lin et al., 1990), while spreading segment centers generally occur at local depth minima and correspond to low MBA values. General categories of ridge axis discontinuities include transform faults (1st order), overlapping spreading centers (OSCs) or non-transform

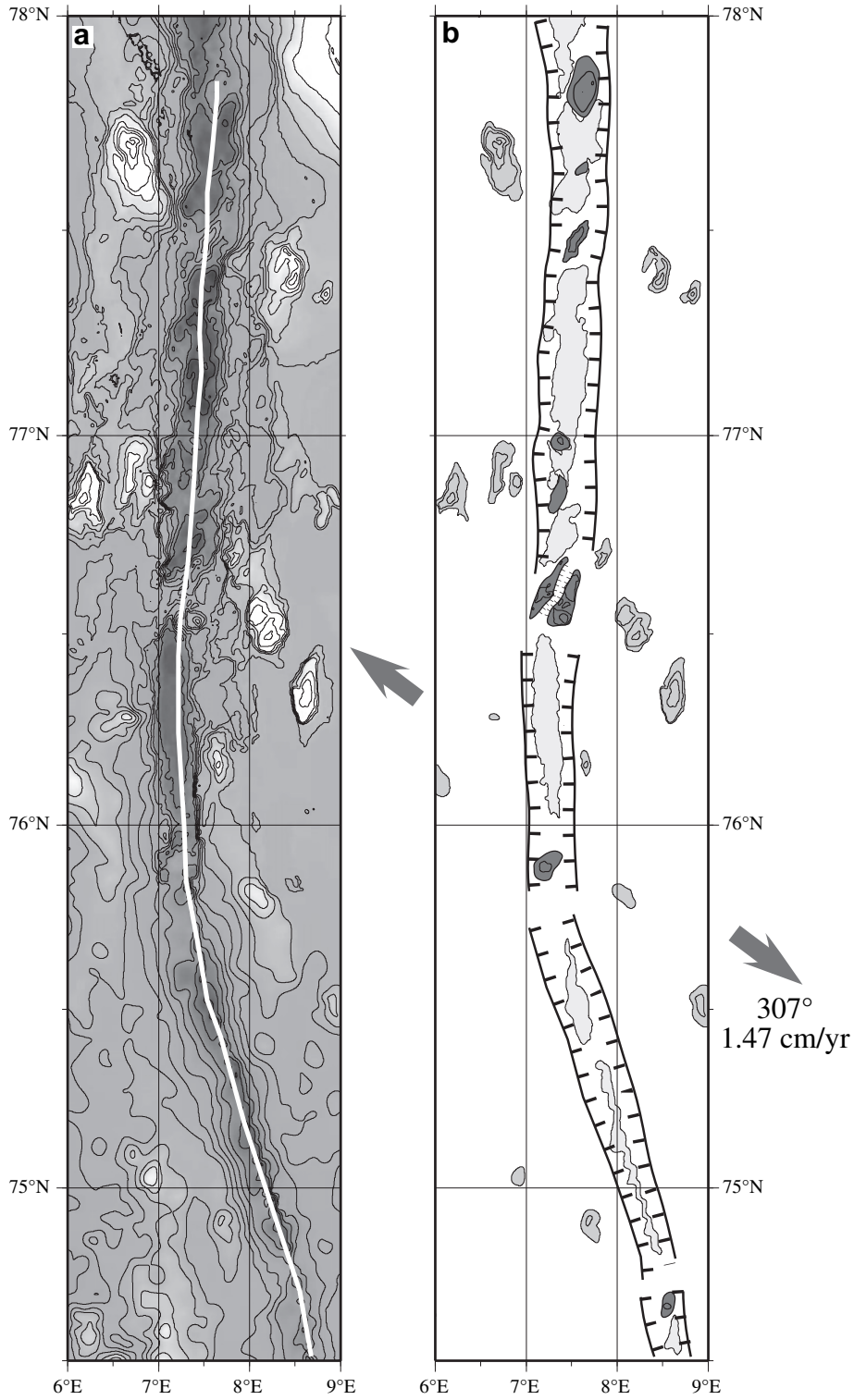

Fig. 2. a) Compiled IBCAO, SeaMARCII, 7.5 and 3.5 kHz echo-sounder data from the Knipovich Ridge axis and near axis crust. Track line is shown in white. Contour interval is 200 m. b) Interpretation showing the location of the rift valley walls (hatched), oblique, en echelon axial highs (dark gray) and elongate axial lows (light gray). The axial highs anchor symmetric chains of off-axis highs (medium gray) that are parallel to plate motion (arrows).

discontinuities (NTDs) (2nd order), and deviations from axial linearity (DEVALs), small OSCs, or other minor discontinuities (3rd order) (Macdonald et al., 1988, 1991; Macdonald, 1982).

Bathymetric data from the Knipovich Ridge indicate that axial highs take the form of isolated en echelon ridges whose long axes are approximately perpendicular to the plate motion direction (Fig. 2a and b). Off-axis seamount chains aligned parallel to plate motion meet the ridge at several of these en echelon axial highs. Similar features and relationships are identified on the Mohns Ridge, the Reykjanes Ridge, and the Southwest Indian Ridge (Murton and Parson, 1993; Géli et al., 1994; McAllister et al., 1995; Dauteuil and Brun, 1996; Tuckwell et al., 1996; Searle et al., 1998b;

Abelson and Agnon, 2001; Sauter et al., 2002). The Knipovich Ridge is uninterrupted by transform faults, however available bathymetric and gravity data have been interpreted to indicate the presence of seven magmatically strong (1st or 2nd order?) and seven magmatically weak (2nd or 3rd order?) segments (Fig. 3, after Okino et al., 2002 and references therein). Four of the magmatically robust segments fall at the intersection between the rift valley and linear chains of off-axis seamounts. This segmentation scheme correlates well with the identified magnetic anomaly pattern and the locations of proposed discontinuities. This segmentation scheme must be considered tentative, as bathymetric, gravity and magnetic data for the Knipovich Ridge are still quite sparse.

Previous investigations using SeaMARCII surface-tow side-scan sonar shows that the axial valley is heavily faulted in orientations oblique to both the ridge and the spreading direction (Crane and Solheim, 1995; Crane et al., 2001). These studies reveal faults that are commonly sigmoidal in plan view, with fault ends sub-parallel to the rift valley walls and the central segments of faults nearly perpendicular to plate motion. These results are similar to fault patterns identified on the Mohns Ridge (Dauteuil and Brun, 1996), in the Gulf of Aden (Dauteuil et al., 2001), and along the Southwest Indian Ridge (Sauter et al., 2002; Dick et al., 2003; Standish et al., 2008).

1.3. Fault populations, dike intrusion, and tectonics

Fault populations at mid-ocean ridges reflect the interplay between tectonic and magmatic forces (plate motion, faulting, dike intrusion), lithospheric rheology (crustal architecture, thermal profiles, strength/depth relationships), and the geomorphic effects of mass wasting and/or resurfacing. Disentangling these disparate influences on the structural character of the ridge axis is critical for understanding relationships between measurable fault parameters and the various forces that shape the axial seafloor. High-resolution bathymetric and sonar imaging of various mid-ocean ridge axes combined with statistical, theoretical and experimental analyses of faults and fault populations have helped clarify the understanding of fault growth and fault population evolution in these extensional environments (Murton and Parson, 1993; Cowie et al., 1994; McAllister et al., 1995; Tuckwell et al., 1996; Searle et al., 1998a; Bohnenstiehl and Kleinrock, 1999, 2000; Gràcia et al., 2000; Parson et al., 2000).

Investigations of fault populations in experiments and in continental and oceanic rifting environments have shown how fault populations change with the angle between plate separation direction and rift trend (Clifton et al., 2000; Clifton and Schlische, 2001, 2003), increasing magnitude of extension (Cladouhos and Marrett, 1996; Ackermann et al., 2001), plate boundary geometry and kinematics (Abelson and Agnon, 1997, 2001; Basile and Brun, 1999), mechanical characteristics of the lithosphere (Ackermann et al., 2001), and in response to dike intrusion events (Rubin and Pollard, 1988; Rubin, 1992, 1995; Ebinger et al., 2008).

The Knipovich Ridge provides an ideal tectonic setting for analyzing the interplay between oblique spreading, ridge segmentation, dike intrusion, and faulting. The balance between magmatic and tectonic influences on the seafloor geology should be very different between volcanic centers and segment ends, especially considering the extremely slow spreading rate and high angle between the ridge and plate motion. Where magmatism is predominant, the impact of dike intrusion on the surficial expression of plate separation should be most clearly displayed, as faults generated during dike intrusion events have been shown to occur generally parallel to dike trend, irrespective of the overall orientation of the rift (Rubin and Pollard, 1988; Rubin, 1992, 1995; Ebinger et al., 2008). At segment terminations, the effects of mechanical stretching should dominate the character of the seafloor, and fault orientations should reflect the interplay between rift trend, extension direction, and the balance between distributed and/or focused deformation (Clifton et al., 2000; Clifton and Schlische, 2001, 2003; Schlische et al., 2002).

The ultra-slow spreading rate should result in extremely low dike intrusion frequency, highlighting and isolating the structural impacts of dike intrusion events at segment centers (Curewitz and Karson, 1998; Wright, 1998). Thus this oblique-, ultra-slow-spreading environment provides an opportunity to discriminate between "magmatically driven" (i.e. dike intrusion driven, roughly perpendicular to plate motion irrespective of ridge trend) and "tectonically driven" (i.e. stretching controlled, oblique to both plate motion and ridge trend) fault populations.

In this paper, we present quantitative fault population data derived from analysis of high-resolution deep-tow side-scan sonar collected along ~400 km of the Knipovich Ridge axis. Our study combines structural analyses with along-axis bathymetry, gravity, and segmentation patterns in order to understand along-axis changes in fault populations. This analysis highlights the impact of ridge orientation relative to plate motion on the geometry and intensity of faulting in different structural settings along the ridge axis.

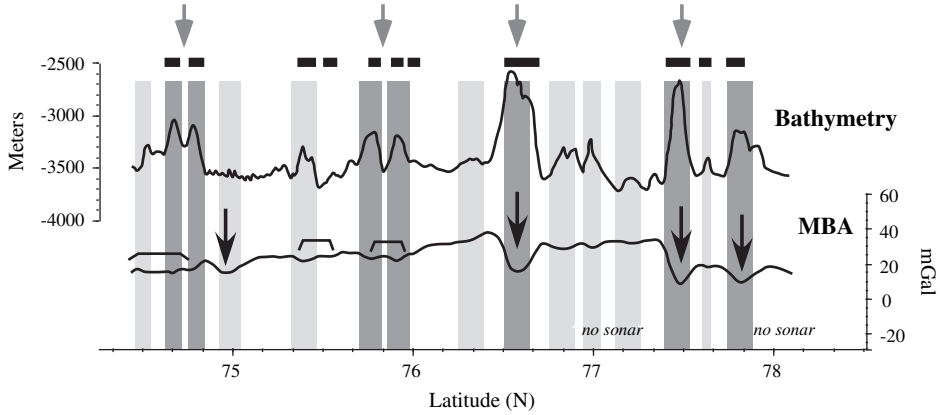

Fig. 3. Along-axis bathymetric profile (top) with identified spreading segments – dark gray vertical bars indicate robust segments anchoring off-axis seamount chains (gray downward-pointing arrows); light gray vertical bars indicate smaller, weaker segments; black boxes mark seafloor dominated by hummocky lava flows and pillow ridges identified in sonar records. Corresponding mantle Bouguer anomaly (MBA) profile (bottom) shows lows (black arrows and brackets) beneath identified segment centers.

2. Data and analytical methods

In fall 2000, we collected ~400 km of 30 kHz side-scan sonar data along the rift axis of the Knipovich Ridge using the ORETech system on the *R/V Professor Logachev* (VNIIO, St. Petersburg, Russia). The sonar device was towed along the ridge at depths ranging from 50 to 150 m above the seafloor, and navigated using an ultra-short-baseline (USBL) transponder system combined with a pressure gauge mounted on the tool. Sonar data were processed on board, and the resulting ~2.5-km-wide images have resolution ranging from ~5 to ~10 m per pixel. These data were interpreted to create detailed structural maps of the axial region.

Faults were identified based on: 1) linear high-reflectance features cutting across lower reflectance regions, 2) linear acoustic shadows obscuring or hiding bottom morphology and 3) disruptions or offsets in geological or morphological features (Fig. 4a). Fault traces were interpreted using commercially available graphics software, and the resulting digital fault trace maps were analyzed using the public domain image processing programs NIH Image (developed at the U.S. National Institutes of Health and available on the Internet at http://rsb.info.nih.gov/nih-image/) and Object Image (available at http://simon.bio.uva.nl/object-image.html). Due to the length of the survey line, the complete sonar image and the corresponding structural interpretation are impossible to reproduce at legible resolution. The fault interpretation map is available as a digital file upon request to the corresponding author.

The structural data consist of: 1) fault trace length – the total length of the fault scarp, 2) tip-to-tip length – the straight line distance between fault trace terminations, 3) fault tortuosity – fault trace length divided by tip-to-tip length, 4) fault azimuth, 5) fault density – total fault length divided by map area, and 6) fault number – total number of faults divided by map area (Fig. 4b).

Fault orientations were interpreted in terms of the angle between the fault and the plate motion vector (Fig. 4c). It must be stressed that any kinematic interpretations of fault motion based on fault orientation have not been verified or ground-truthed using offset markers, fault-plane kinematic indicators, or piercing points. While there are investigations showing that kinematic inferences may be supported by theoretical, experimental, and observational analyses relating stress state, fault/fracture orientation, fault slip vector and local strain (Reches and Dieterich, 1983; Reches, 1983; Chiotis and Tsoutrelis, 1992; Dupin et al., 1993), our interpretation of fault orientation data is limited to fault strike only. Faults are designated as perpendicular, sub-perpendicular, oblique, sub-parallel, and parallel to plate motion in Fig. 4c and subsequent discussion.

Limitations of our data include the small swath width of the sonar survey, the lack of parallel, overlapping survey lines, and the orientation of the survey line relative to the ridge axis and the dominant fault orientation. These factors limit the sampled fault population: faults at a high angle to the track line and longer than 2.5 km are truncated by the edge of the survey; the population of faults longer than 2.5 km may be biased toward sub-parallelism to the survey line; and clipping or truncation of imaged faults may artificially increase the population of smaller faults. These limitations were considered during interpretation, and faults that were affected by these aliasing, clipping and censoring effects were 1) very low in abundance relative to the number of fully imaged fault segments, and 2) accounted for (by removal) during analysis of the fault population.

In the following sections, the fault data are analyzed as a set comprising the entire ridge, as two subsets based on the change in axial trend at 75°50′N, and finally subdivided using an along-axis sub-sampling of the fault population conducted using a 10-km-long moving window (selected based on the requirement to sample the

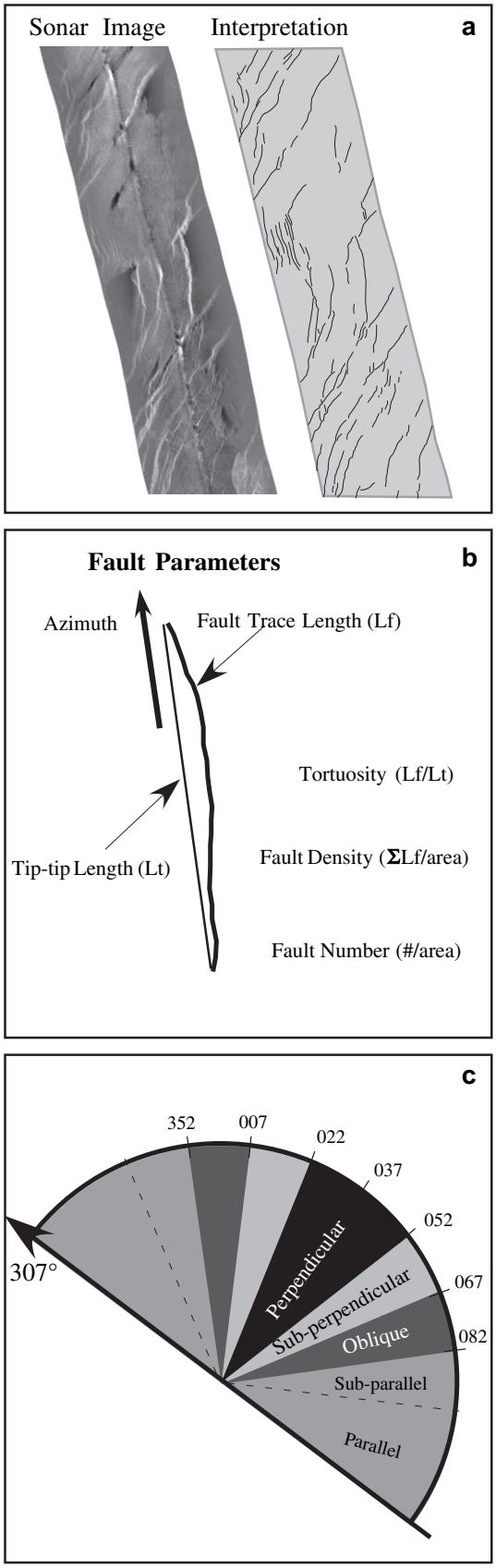

Fig. 4. a) Example sonar image and fault trace interpretation map. b) Parameters measured for structural analysis. c) Classification of fault trace strike relative to plate motion (arrow, 307°).

longest faults without clipping) stepped down the ridge at intervals of 1 km. The along-axis data were compared to the depth profile of the ridge measured using the shipboard 3.5 kHz and the ORETech 7 kHz sub-bottom profiler, and to the segmentation pattern discussed previously.

3. Results

3.1. Fault population measurements and statistics: all data

The survey conducted in the fall of 2000 comprises a narrow, high-resolution glimpse of a long portion of the central regions of the axial valley of the Knipovich Ridge. Approximately 4500 faults were measured. Measuring and analyzing the fault data over the entire ridge enables characterization of the small-scale, youngest structures present in the plate boundary zone.

3.1.1. Fault trace length and tip-to-tip length

Fault lengths measured in this study range from 22 to 2750 m, with a characteristic length of ~340 m (as discussed below, the fault population measured in this survey exhibits an exponential relationship between number and length, requiring the use of characteristic length rather than mean length, where the characteristic length is the inverse of the exponent describing the fault population). Tip-to-tip length (the straight line distance between fault terminations, see Fig. 4b) ranges from 10 m to 2520 m, with the same characteristic length. There is a strong positive correlation ($R^2 = 0.99$) between fault length and tip-tip length. Based on the resolution limits of the sonar data (5–10 m per pixel), and the uncertainties involved in sonar interpretation of fault scarps and fault-line scarps, the differences between fault trace length and tip-to-tip length are considered insignificant and well within measurement error. Therefore, all fault length data are presented using only the measured fault trace length.

3.1.2. Fault tortuosity

The tortuosity of measured faults is determined by dividing fault length by tip-to-tip length. Tortuosity is a dimensionless value that describes the curvature per unit length of the fault trace (after Clifton et al., 2000). The minimum value for tortuosity is 1.0, indicating a perfectly straight fault, and the maximum value is (theoretically) infinite. Tortuosity of faults imaged along the Knipovich Ridge axis ranges from 1.02 to 2.19. There is little or no correlation between tortuosity and fault length. As stated above, given inherent resolution and measurement errors, there is little or no meaningful difference between the fault trace length and tip-to-tip length in this data set. Tortuosity data were calculated and correlations between tortuosity, length, and azimuth were investigated, however, because tortuosity is not considered a reliable fault parameter, these data are excluded from this analysis.

3.1.3. Fault azimuth

Fault azimuths were measured by determining the orientation of the straight line connecting fault terminations. All azimuths are determined based on orientations in the top half of the compass rose, centered on North. Azimuths range from 270° to 082°, with a mean of 013°, median of 014°, and mode of 012°. The skewness of the azimuth data is −0.2, indicating a near normal distribution around the mean (Fig. 5b).

A comparison of fault length and fault azimuth indicates that faults longer than 1000 m have a mean azimuth of 021°, range in azimuth from 295° to 057°, and comprise ~4% of the fault population. In contrast, faults shorter than 1000 m have a mean azimuth of ~013°, range in azimuth from 271° to 082°, and comprise ~96% of the fault population (Fig. 5c).

Dividing the data into two sub-populations based on the change in axial trend at 75°50′N reveals a distinct change in fault strike between the northern (Fig. 5d) and southern sections of the ridge (Fig. 5e). The northern section exhibits a single, normally distributed population with a mean strike of ~014°. In contrast, the southern section exhibits a bimodal distribution of fault strike with peaks at ~015° and at ~245°, and a mean of ~011°.

3.1.4. Fault-scaling

Faults measured along the Knipovich Ridge exhibit an exponential relationship between the number of faults greater than or equal to a given length ($N \geq L$) and fault length (in kilometers), with an exponent of −2.95 and an R^2 line fit of 0.994 (Fig. 6a). When the longest faults and shortest faults are removed from the data set, to account for clipping and resolution limitations, there is little change in either the slope (−2.84) or the fit ($R^2 = 0.993$) of the exponential relationship between length and number of faults.

Analysis of the fault-scaling relationships found in the Crane et al. (2001) sonar survey reveals a fault population that has similar R^2 curve fits for both exponential ($R^2 = 0.92$, exponent = −0.091) and power-law ($R^2 = 0.89$, exponent = −1.55) relationships between length and number (Fig. 6b). The differences between the scaling relationships found in the narrow, high-resolution and in the wide-area, lower-resolution surveys may be related to the scale of observation: significant numbers of smaller faults will not register in the wide-area survey, and longer faults with wider spacing will not register in the narrow, high-resolution survey. Alternatively, assuming that sampling bias is not completely responsible for these differences, the variation in scaling relationships between the two surveys may reflect differences in the thickness or strength of the lithosphere as measured at the center of the rift valley in contrast to the entire rift valley, as discussed in more detail below.

3.2. Along-axis variations

We used a 10-km-long moving window stepped down the ridge axis at intervals of 1 km in order to extract and measure changes in fault population parameters along the length of the Knipovich Ridge (Fig. 7). These parameters include characteristic length, fault azimuth, fault density, and fault number. Fault number and fault density are strongly correlated, so only fault density is plotted in the along-axis profile in Fig. 7.

Fault density (the sum of fault lengths over a given area of measurement) (Fig. 7a) varies between 0.4 and 2.9 km/km^2, with a mean of 1.72 and standard deviation 0.57 km/km^2. Characteristic fault length (Fig. 7b) varies significantly over the length of the ridge axis, from minimum values of 130 to maximum 570 m. Mean fault azimuth (Fig. 7c) ranges between 335° and 033°, averaging 013° with standard deviation 7.3°. We subdivided the fault population in each sampling window into four categories (as discussed in Section 2 and shown in Fig. 4c) determined by the geometric relationship between the fault trace and the NUVEL-1A/REVEL predicted plate motion vector of ~307°. All parameters are plotted with respect to the axial bathymetric and MBA profiles (after Okino et al., 2002) (Fig. 7d and e).

3.2.1. Segment centers

Volcanic axial highs, distinct MBA lows, and highly reflective hummocky bottom morphology characterize Knipovich Ridge spreading segment centers (Fig. 8a). These areas are marked by locally higher average fault lengths and fault density is locally low. Elongate pillow mounds whose long axes trend near perpendicular to plate motion are the dominant form of volcanic construction in these areas. Segment centers are dominated by faults striking perpendicular to plate motion (35–80% of the fault population), with a lesser population striking sub-perpendicular to plate motion

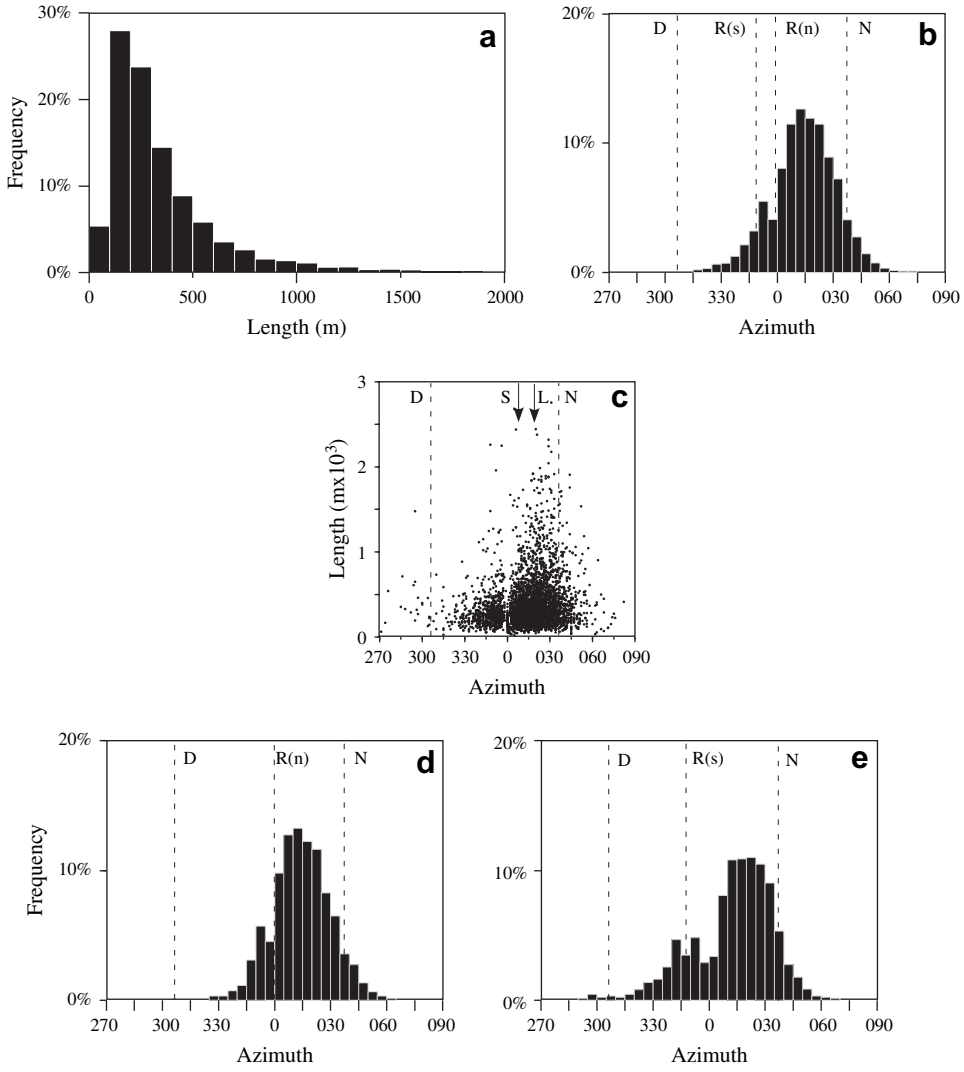

Fig. 5. a) Histogram of fault lengths. b) Histogram of Fault Azimuth (D - displacement direction; *R*(*s*), *R*(*n*) – ridge trends, southern and northern sections, respectively; *N* – plate motion normal). c) Fault Length vs. Fault Azimuth (S – mean azimuth for faults <1000 m; L – mean azimuth for faults > 1000 m). d) Histogram of Fault Azimuth, northern section of the Knipovich Ridge (alpha ~53°). e) Histogram of Fault Azimuth, southern section of the Knipovich Ridge (alpha ~40°).

(20–30%), and small populations of faults striking sub-parallel (<15%) or parallel (<5%) to plate motion.

3.2.2. Segment ends

Bathymetric lows characterized by heavy sediment cover, gravity highs, and low-reflectivity terrain mark segment boundaries (Fig. 8b). These areas are marked by locally lower average fault length and fault density is locally high. Fault populations in these areas along the Knipovich Ridge exhibit characteristics that are distinctly different from populations found on axial highs. Faults striking perpendicular to plate motion make up less than 25%, sub-perpendicular faults comprise 40–60%, sub-parallel faults make up 25–50%, and parallel faults comprise 5–10% of the fault population.

3.2.3. Steep slopes and mass wasting deposits

Several areas along the ridge axis do not follow the general trends described above. These areas are marked by chaotic reflection patterns, irregular seafloor fabrics, a much higher percentage of short, straight, highly oblique faults, and very low fault density (Fig. 8c). These sites are found along areas of the ridge axis with steep slopes, generally on the margins of volcanic axial highs. Investigation of these sonar images and fault characteristics suggests that these are sites of submarine landslides or mass wasting deposits, and that the faults interpreted in these areas cannot be directly related to either tectonic or magmatic activity without further, more detailed investigation.

4. Discussion

4.1. Oblique extension: terminology and components

Investigations of extension in areas where rifts and/or spreading ridges are not perpendicular to the plate motion direction have given rise to a set of descriptive variables delineating the geometry. The overall trend of the rift or ridge (*R*) is compared to the displacement direction (D), and the angle between them is described by the angle alpha (α) (after Withjack and Jamison, 1986). In this investigation, the displacement direction is taken to be the plate motion vector, determined using global positioning and geodesy (Sella et al., 2002). We define the term "obliquity" of the ridge by subtracting α from the normal to the ridge trend ($90 - \alpha$). Abelson and Agnon (1997) described the angular difference between second-order segments and overall ridge trend as "discordance" (β), and we parallel this in our investigation by

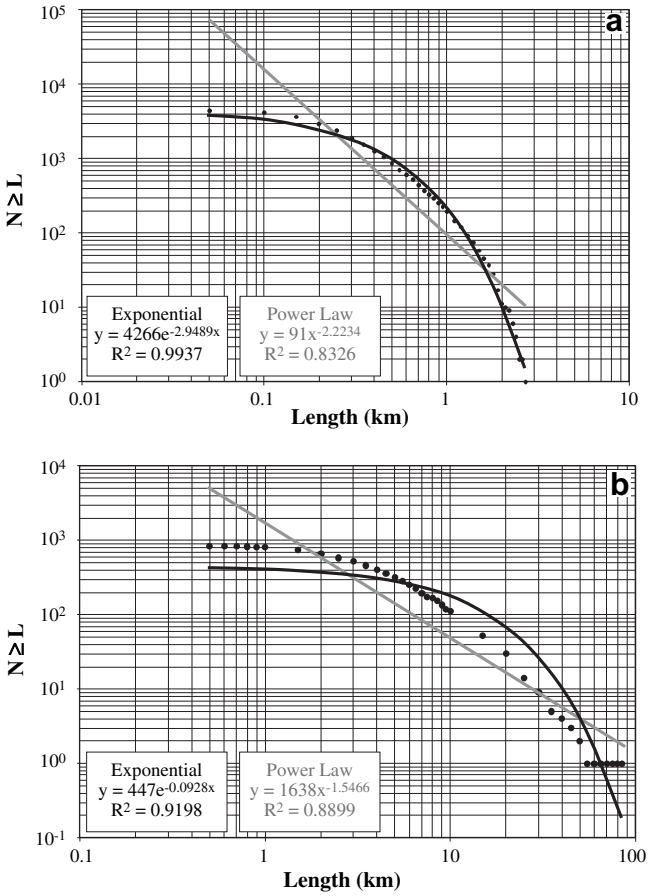

Fig. 6. a) Logarithmic length–cumulative number plot for the high-resolution ORETech sonar fault data showing the relationship between number of faults greater than a given length ($N(L) \geq L$) and length (km). The best-fit relationship is an exponential curve with exponent ~2.95, indicative of low strain and/or low effective elastic thickness. b) Similar diagram for the lower-resolution SEAMARCII fault data (from Crane et al., 2001) showing an ambiguous or transitional relationship between number and length, with nearly equal R^2 values for both exponential (−0.098) and power-law (−1.55) slopes.

determining the difference between mean fault strike and the ridge trend using the term ψ. In obliquely spreading systems the plate motion vector and the incremental extension direction (represented by faults) are not necessarily synonymous. Where the ridge is perpendicular to plate motion ($\alpha = 90°$), the incremental extension direction is generally parallel to displacement. As α decreases and the ridge is progressively more oblique to the spreading direction, incremental extension is no longer parallel to plate motion. Instead, incremental extension occurs at an angle to both the displacement direction and the rift normal. Our analysis focuses on measuring the orientation of faults as markers of incremental extension and comparing those orientations along the ridge in different local magmatic/tectonic settings. The angular differences between mean fault orientations as compared to the ridge trend along ridge segments with different orientations, and along relatively magma poor vs. magma rich portions of the ridge should reflect changes in local response to extension driven by oblique rifting and/or extension driven by magmatic activity (i.e. dike intrusion at depth).

4.2. Fault populations and oblique spreading

Analyses of oblique spreading and ultra-slow spreading centers (Dauteuil and Brun, 1993, 1996; Murton and Parson, 1993; Géli et al., 1994; Taylor et al., 1994; McAllister et al., 1995; Tuckwell et al., 1996; Searle et al., 1998b; Klingelhöfer et al., 2000; Dauteuil et al., 2001; Sauter et al., 2002; Dick et al., 2003; Standish et al., 2008) show that they are characterized by 1) faults oblique to both the rift walls and to the opening direction, 2) population variability between normal, oblique, and strike-slip faulting, depending on location within the rift system, and 3) extreme variations in the geometry and distribution of axial volcanic edifices. The geometry of faults and the spatial distribution of faults with different geometries in oblique rifts are dependent on the angle between the ridge and the spreading direction (Clifton et al., 2000; Clifton and Schlische, 2001, 2003), and possibly the presence of an underlying magma body (Mart and Dauteuil, 2000). Fault population characteristics are also influenced by the amount of extension, the effective elastic thickness of mechanically strong layers, and the strain rate (Cladouhos and Marrett, 1996; Ackermann et al., 2001). Analysis of side-scan sonar data (Sauter et al., 2002) and geophysical/geochemical data (Standish et al., 2008) shows that the interplay between magmatism, faulting and oblique spreading gives rise to similar systematic variations between axial morphology, basalt chemistry, MBA anomalies, and structural geology along the Southwest Indian Ridge.

The fault populations and axial volcanic features measured along the center of the Knipovich Ridge highlight similar relationships. Average fault orientation is oblique to both the rift axis and to the spreading direction, and fault orientation varies in concert with axial segmentation and morphology. Faults are generally short and fault-scaling parameters are exponential in the axial region, reflecting a low degree of extension (i.e. <5%) and (presumably) a relatively thin mechanically strong layer in the axial region (after Cowie et al., 1994; Dawers and Anders, 1995; Cladouhos and Marrett, 1996; Ackermann et al., 2001). It cannot be ruled out that the fault population characteristics of this spreading center are reflective of its highly oblique character (e.g. Clifton et al., 2000), rather than an indication of degree of extension or thickness of the mechanically competent layer. However, variations in fault-scaling relationships between the axial region and the rift valley as a whole, demonstrated by the contrast between this survey and Crane et al. (2001) data, suggest that there is some significance to the exponential character of the fault population in the axial region.

In contrast, faults measured using long-range, wide coverage side-scan sonar (data from Crane et al., 2001) are generally longer (mean 5700 m) and exhibit fault-scaling relationships that appear transitional between exponential and power-law. These contrasts, while there is most likely a strong dependence on measurement scale and resolution, may reflect differences between the character of the lithosphere in the center (thinner, hotter, weaker) and the margins of the axial region (thicker, colder, stronger).

In experimental models and field studies, the difference between the rift trend (R) and the opening direction (D) is defined as the parameter α, which can be used to derive the obliquity ($90 - \alpha$) between the spreading direction and the rift normal (after Clifton et al., 2000). In systems with known obliquity, there is a near-linear relationship between mean fault azimuth (az) and rift obliquity (Fig. 9, after Clifton et al., 2000; Clifton and Schlische, 2001, 2003).

For the purposes of constructing Fig. 9, we used $90 - \alpha$ to represent obliquity. Using mean fault azimuth data and the trend of the Knipovich Ridge rift valley walls, we attempted to reproduce the plate motion direction between Eurasia and North America. Mean fault strike along the Knipovich Ridge (014° in the north and 011° in the south) was compared to the ridge trend (~000° in the north and ~347° in the south) to derive the angular difference between the mean fault azimuth and the ridge trend (ψ in Fig. 9, analogous to "discordance" or β in Abelson and Agnon, 1997). These values were used to calculate the "predicted obliquity" ($90 - \alpha$)

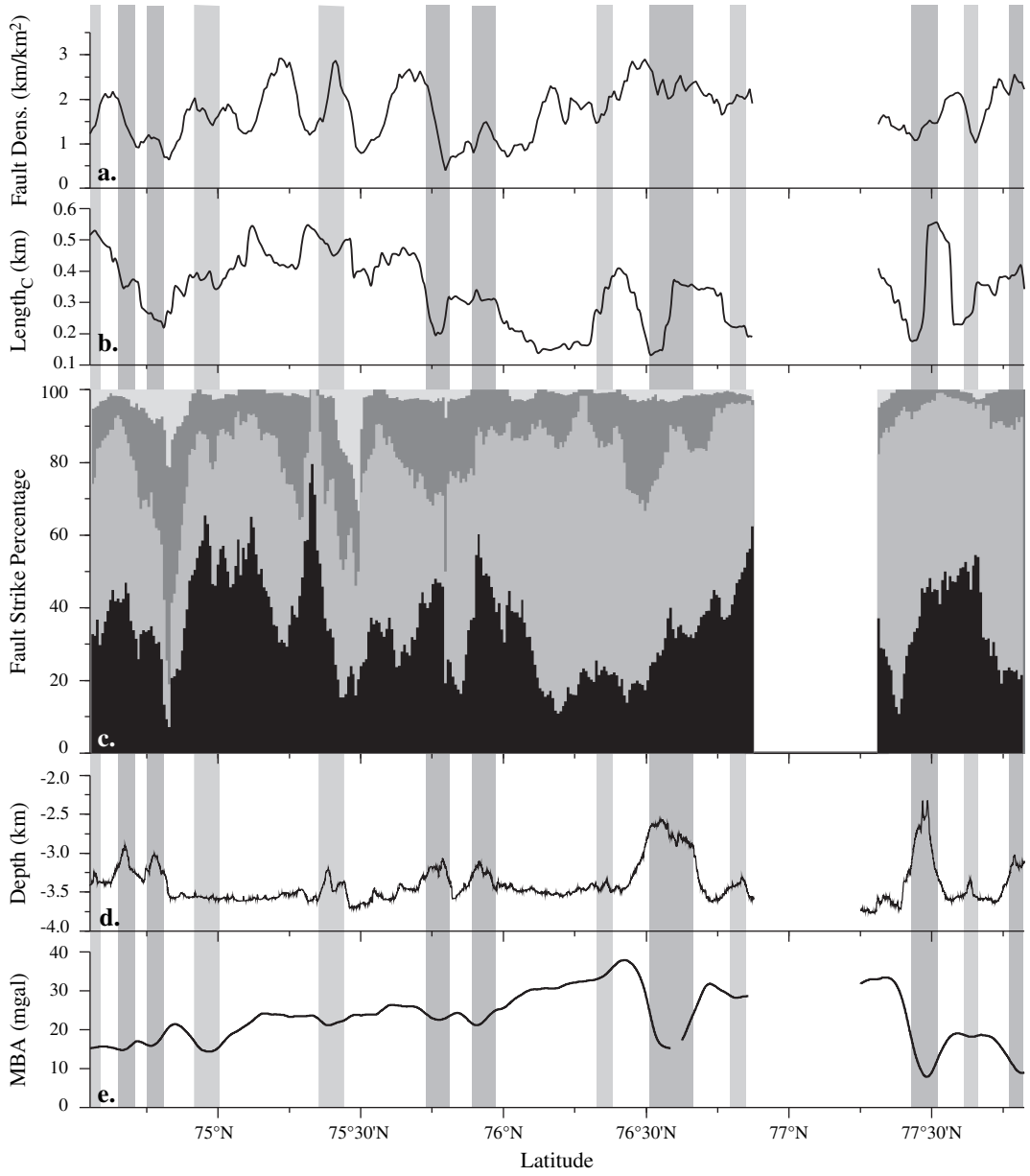

Fig. 7. Along-axis plots of fault parameters compared to axial segmentation (dark gray boxes – robust segments, light gray boxes – weaker (or inferred) segments). a) Fault Density – sum of fault lengths divided by a given area. b) Characteristic length (Length$_C$) of exponential fault population. c) Fault Azimuth populations grouped according to strike relative to plate motion (see text and Fig. 4c for explanation). Black: perpendicular, medium gray: sub-perpendicular, dark gray: oblique, light gray: sub-parallel and parallel. d) Axial depth profile. e) Axial mantle Bouger anomaly profile. The lack of data between 76°50′N and 77°10′N is a consequence of technical difficulties during the expedition.

based on the best-fit line to the experimental data from Clifton et al. (2000), and a "predicted plate motion" by adding this derived α to the ridge axis normal (N). The values for $90-\alpha$ derived from this exercise are 30° in the north, and 43° in the south, resulting in plate motion vector orientations of ~300° for both ridge sections, within 7° of the NUVEL-1A and REVEL predictions of ~307°. Undertaking the same calculations using data from field studies of Iceland (Clifton and Schlische, 2003) and analyses of other oblique rifting environments (Clifton et al., 2000) gives similar results, indicating that fault strike may be an accurate predictor of plate motion direction, even in oblique rift settings.

One important detail to note is that in both the experimental and observational analyses of fault populations in rifts (Clifton et al., 2000; Clifton and Schlische, 2001, 2003), starting at α of 30° (obliquity of 60°) to progressively lower values of α (greater obliquity), a bimodal fault population develops with one set of displacement-perpendicular and a second set of displacement parallel faults. This phenomenon may explain the differences between the northern and southern Knipovich fault populations discussed earlier. The best-fit line in Fig. 9 (bottom) is based on the population of faults closest to perpendicular to plate motion (denoted by the dashed line segment), showing that even in highly oblique settings where fault populations are bimodal, one of the subsets of the fault population still conforms to the prediction that obliquity and fault orientation are inextricably linked.

4.3. Along-axis variations – influence of axial segmentation

Fault populations along mid-ocean ridges are affected by many surficial modification processes, including mass wasting, landslides, sedimentation, lava flow carapace collapse, and resurfacing

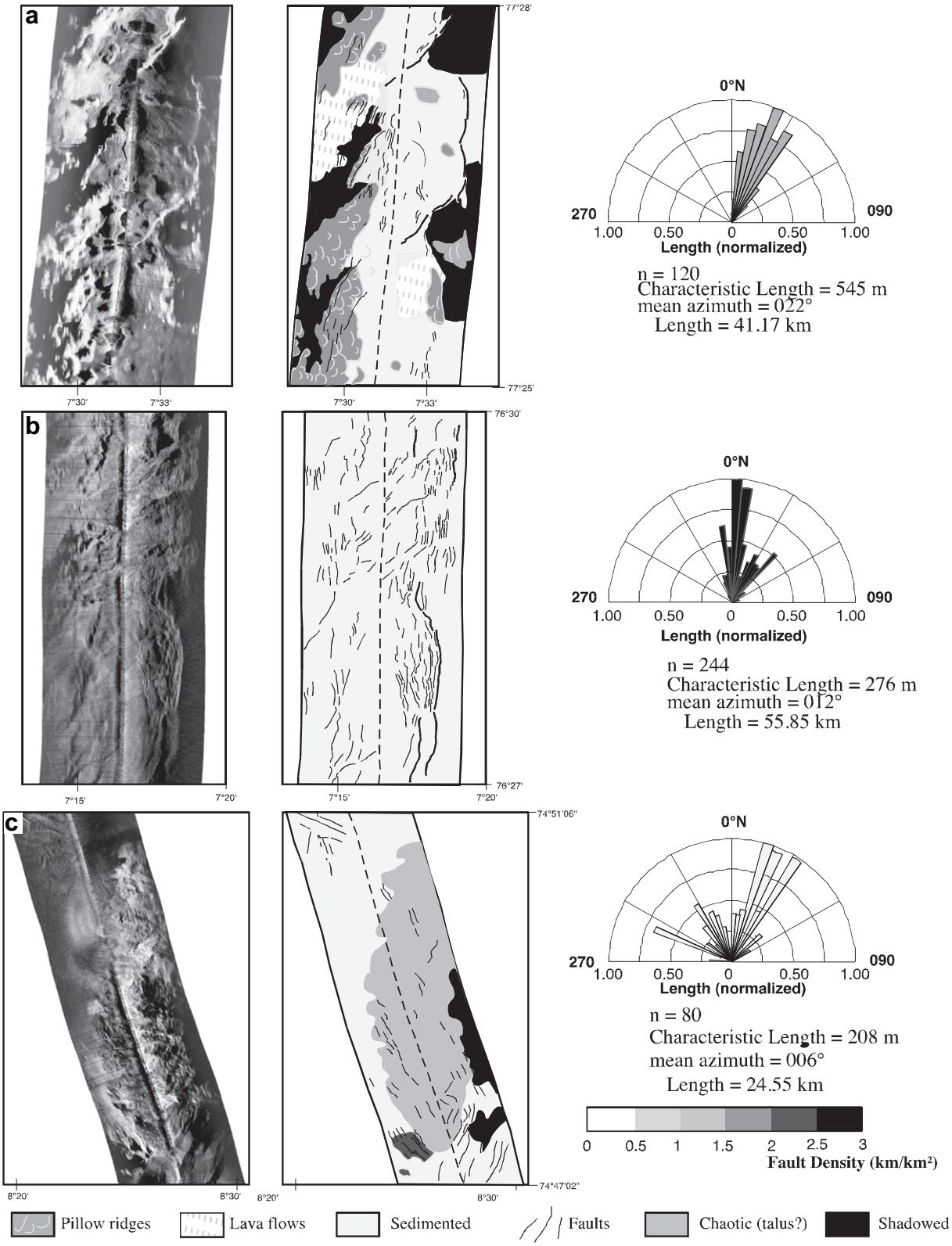

Fig. 8. Examples of sonar records (left), geological and structural interpretations (middle), and length-normalized rose diagrams of faults with pertinent fault population data (right). a) Volcanic axial high with linear, hummocky volcanic mounds, long normal faults, and shorter oblique faults. b) Axial depression with large numbers of short oblique faults, and no volcanic material. c) Mass wasting feature found on the flank of a large axial volcano; faults have widely scattered strikes, short lengths, and low fracture density.

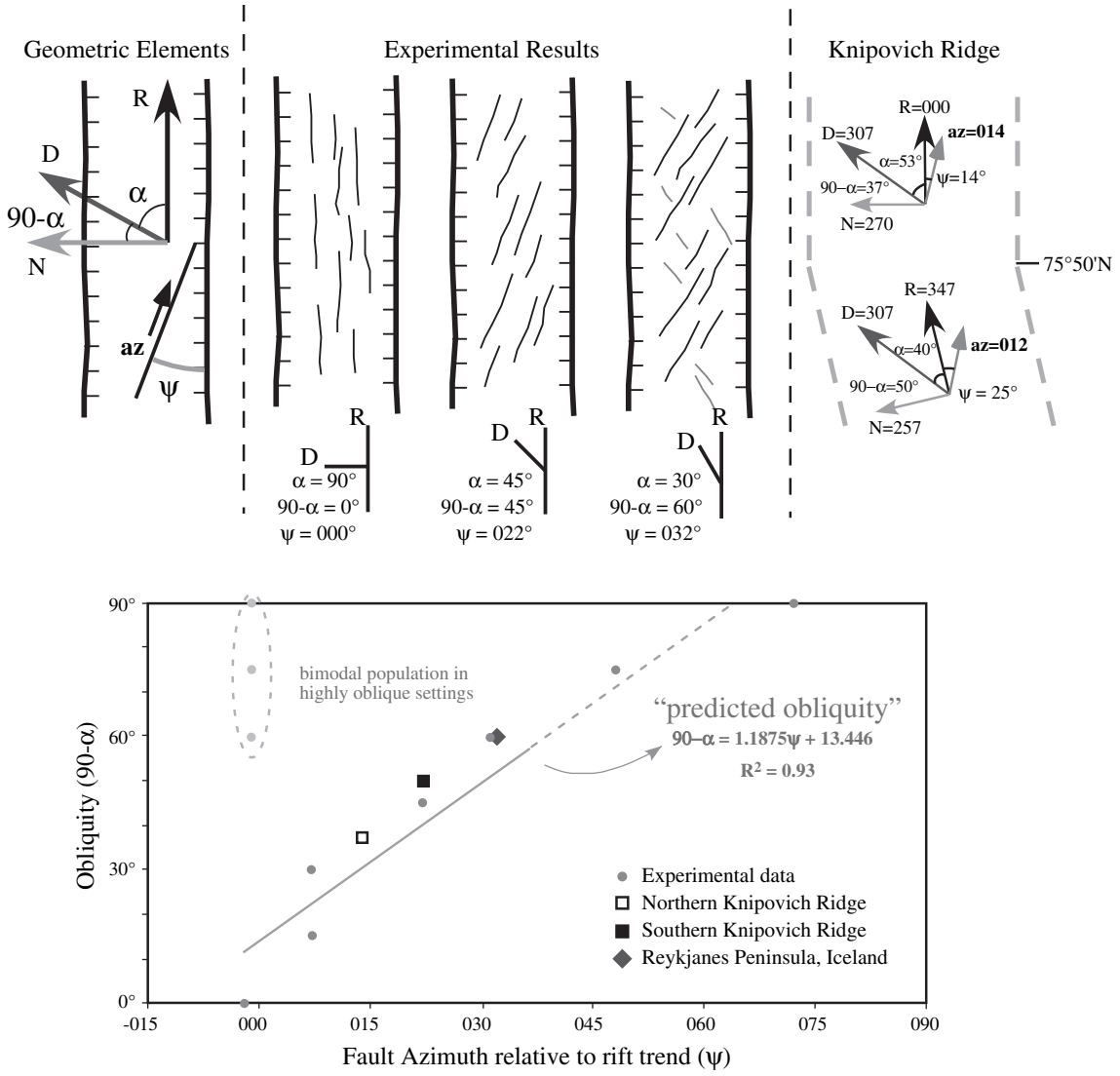

Fig. 9. Top left – schematic: components of oblique rifting: *R*, rift axis; D, plate motion, *N*, normal to rift; angle between ridge trend and plate motion is α ($R - D$), obliquity is $90 - \alpha$, or $N - D$; **az**, mean fault azimuth; ψ, mean fault orientation relative to rift (**az**-*R*). Top center – schematic diagrams showing the systematic relationship between mean fault orientation relative to rift trend (ψ) as a function of changing angle between spreading and rift trend (α) (analogous to obliquity ($90 - \alpha$)) from experimental data (after Clifton et al., 2000). Top right – geometry and values for these elements along the northern and southern Knipovich Ridge. Bottom – plot of ψ vs. $90 - \alpha$ with line fit to experimental data, observational data from Iceland and this study. Observational data fall close to the experimental trend resulting in obliquity predictions ($90 - \alpha$, derived from the best-fit line) of ~30° and ~43°, respectively. Predicted plate motion derived from these data, where $D = N + (90 - \alpha)$, are both ~300°, within seven degrees of the relative plate motion predicted by the NUVEL-1A and REVEL global plate motion models (DeMets et al., 1990, 1994; Sella et al., 2002). See text for discussion.

by new lava flows. Since these processes operate over a wide range of geologic time periods at a given location, any image of the sea bottom is a time-integrated snapshot of the local surficial geology. With these caveats in mind, we discuss the along-axis comparison of fault populations to axial segmentation.

When the fault population data are broken down into along-axis sub-regions, the relationship between fault azimuth, fault length, fracture density and the axial depth profile sheds light on the interplay between structural and magmatic influences on fault population parameters (Fig. 10). Elongate, en echelon axial highs have long axes near perpendicular to plate motion and are marked by evidence (from sonar, camera and sampling) for recent volcanism (Fig. 8a). Volcanic construction on these axial volcanic ridges is characterized by chains of hummocky pillow ridges (that yielded fresh, glassy basaltic pillow samples) trending approximately perpendicular to plate motion, similar in character and occurrence to features observed above sites of recent dike intrusion (Head et al., 1996; Chadwick et al., 1995, 2001; Chadwick and Embley, 1998). Faults in these areas are nearly perpendicular to plate motion, relatively long and widely spaced, resembling faults related to dike intrusion events both on land and in submarine environments (Rubin and Pollard, 1988; Chadwick and Embley, 1998; Ebinger et al., 2008). We infer that dike intrusion is the dominant mechanism controlling the character of the fault population in these areas.

In contrast, where the ridge axis is deep, there is little evidence for recent volcanism, and sonar data and core sampling indicate that sediments cover the seafloor (Fig. 8b). Faults in these areas are highly oblique to the plate motion direction, relatively short, and closely spaced. These observations suggest that the geometry and mechanics of non-transform discontinuities may reflect the linkage of en echelon fault segments, creating accommodation zones with dense populations of faults that are oblique to the main fault orientation (Peacock and Sanderson, 1991; Vermilye and Scholz, 1999; Tavarnelli and Pasqui, 2000). The geometry, spatial distribution, and density of the fault populations at these inferred

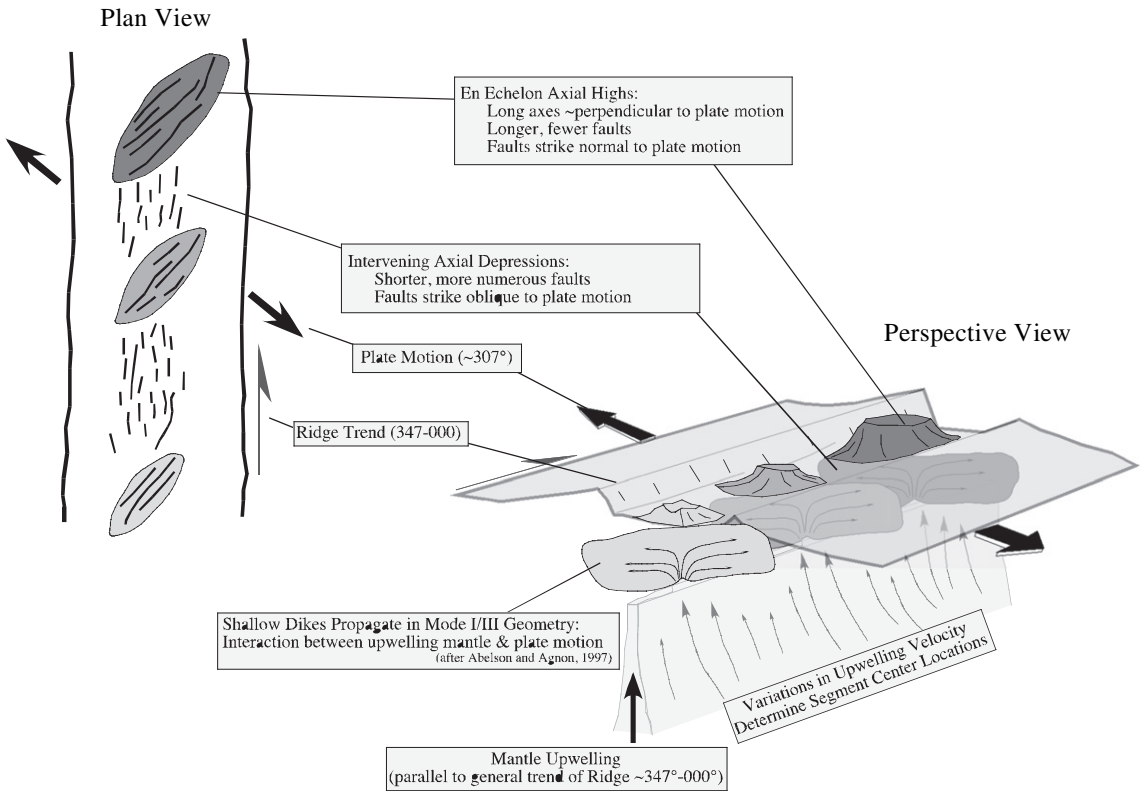

Fig. 10. A model incorporating oblique spreading geometry, dike intrusion, and fault population characteristics along the Knipovich Ridge. The left hand diagram (plan view) is a schematic showing the distribution of en echelon volcanic axial highs (shaded), with fault geometry and structural fabric shown by dark lines. The right hand diagram (perspective view) is a schematic representation of the interplay between magmatic and mechanical spreading. The ridge itself is parallel to the overall mantle upwelling zone, dikes fed from this zone propagate approximately perpendicular to the plate motion direction, forming en echelon axial highs and influencing the fault patterns shown in the plan view of the ridge axis.

segment boundaries may reflect the formation and maintenance of accommodation zones in relatively thicker and colder lithosphere away from the primary sites of magmatic activity.

Sonar and remote imaging surveys of axial regions along the fast-spreading East Pacific Rise (Wright et al., 1995, 2002; Wright, 1998) show strong correlation between fault and fissure densities and orientations, ridge segmentation patterns, and seafloor relative age, in accord with the conclusions drawn from our survey. Analyses of oblique-spreading ridges show relationships between obliquity, segmentation, magma supply and remote driving stresses (Abelson and Agnon, 1997), which mirror experimental results (Clifton et al., 2000; Mart and Dauteuil, 2000; Clifton and Schlische, 2001; Corti et al., 2001) and recent observational results from oblique-spreading environments (Sauter et al., 2002; Clifton and Schlische, 2003). We suggest that these observations, coupled with our analysis, support models of mode I/III propagation of dikes rising from magma chambers or mantle sources beneath oblique spreading centers (e.g. Abelson and Agnon, 1997). These magma sources accumulate above mantle upwelling cells that follow the general trend of the spreading axis, while the dikes that rise from these source regions propagate near perpendicular to plate motion (e.g. Dauteuil and Brun, 1993; Rubin, 1995; Abelson and Agnon, 1997).

As dikes propagate vertically and horizontally, they induce normal faulting at the surface during (Rubin and Pollard, 1988; Rubin, 1992; Chadwick and Embley, 1998; Curewitz and Karson, 1998; Ebinger et al., 2008). A dike intrusion event monitored beneath an en echelon axial high on the oblique-spreading Mohns Ridge (Blackman et al., 2000) propagated near perpendicular to plate motion and oblique to the ridge axis trend. Construction of en echelon axial highs on the Knipovich Ridge by similar dike intrusion events should result in the creation of the observed volcanic and structural features. Lower fracture density and fault number in these areas may reflect resurfacing that accompanies the eruption of lava: older faults may be covered (Chadwick et al., 1995, 2001; Chadwick and Embley, 1998). Alternatively, the wider fault spacing characteristic of segment centers may reflect dike geometry and/or the depth of dike intrusion in the crust (Rubin and Pollard, 1988; Rubin, 1992). The fault length and fault density measurements at segment ends reflect the influence of oblique spreading and/or the structural geometry of accommodation zones. The contrast between segment centers and segment ends is heightened by both the ultra-slow spreading rate (i.e. low dike intrusion frequency) and by the extreme obliquity of this spreading system.

5. Conclusions

Structural analysis of side-scan sonar images from the Knipovich Ridge axis reveals the following relationships:

1. Faults in the axial region are oblique to both plate motion and the ridge axis, consistent with experimental and observational results in oblique extensional environments.
2. Fault length-scaling relationships indicate low extensional strain and/or low effective elastic thickness in the axial region relative to the ridge as a whole.
3. Longer faults are nearly normal to plate motion, while shorter faults have highly variable orientations.
4. Along-axis profiling shows that fault population characteristics vary as a function of local tectonic setting: Volcanic axial highs

(segment centers) host longer, relatively lower-density faults that are perpendicular to sub-perpendicular to plate motion. Conversely, non-volcanic axial depth minima host shorter, relatively higher density populations of faults oriented oblique to sub-parallel to plate motion.
5. Fault populations at en echelon axial highs reflect the influence of dike intrusion on the seafloor fabric.
6. Fault populations in intervening axial lows (segment ends) reflect the geometry and mechanics of oblique extension, accommodation zones, and non-transform discontinuities.
7. Oblique, ultra-slow spreading imparts distinctive, and variable, structural fabric to the axial seafloor. Fault population analysis reveals the influence of different spreading mechanisms on the morphology and geology of the axial region.

Acknowledgements

We are grateful to Amy Clifton, Meir Abelson, Roy Schlische, and an anonymous reviewer for their exhaustive reviews of the manuscript. Data gathering and interpretation were funded by the Japan Society for the Promotion of Science (grant # P99673) and by the Ocean Research Institute, University of Tokyo. Final manuscript preparation supported by the National Science Foundation (Prime Award No. OCE-0222154 Awarded to Duke University, Subaward No. 07-SC-NSF-1040 awarded to Syracuse University).

Appendix. Supplementary data

Supplementary data associated with this article can be found, in the online version, at doi:10.1016/j.jsg.2009.08.011.

References

Abelson, M., Agnon, A., 1997. Mechanics of oblique spreading and ridge segmentation. Earth and Planetary Science Letters 148, 405–421.
Abelson, M., Agnon, A., 2001. Hotspot activity and plume pulses recorded by the geometry of spreading axes. Earth and Planetary Science Letters 189, 31–47.
Ackermann, R.V., Schlische, R.W., Withjack, M.O., 2001. The geometric and statistical evolution of normal fault systems: an experimental study of the effects of mechanical layer thickness on scaling laws. Journal of Structural Geology 23, 1803–1819.
Basile, C., Brun, J.P., 1999. Transtensional faulting patterns ranging from pull-apart basins to transform continental margins: an experimental investigation. Journal of Structural Geology 21, 23–37.
Blackman, D.K., Nishimura, C.E., Orcutt, J.A., 2000. Seismoacoustic recordings of a spreading episode on the Mohns Ridge. Journal of Geophysical Research 105, 10961–10973.
Bohnenstiehl, D.R., Kleinrock, M.C., 1999. Faulting and fault scaling on the median valley floor of the trans-Atlantic geotraverse (TAG) segment, ~26°N on the Mid-Atlantic Ridge. Journal of Geophysical Research 104, 29351–29364.
Bohnenstiehl, D.R., Kleinrock, M.C., 2000. Fissuring near the TAG active hydrothermal mound, 26°N on the Mid-Atlantic Ridge. Journal of Volcanology and Geothermal Research 98, 33–48.
Chadwick, W.W., Embley, R.W., 1998. Graben formation associated with recent dike intrusions and volcanic eruptions on the mid-ocean ridge. Journal of Geophysical Research 103, 9807–9825.
Chadwick, W.W., Embley, R.W., Fox, P.J., 1995. SeaBeam depth changes associated with recent lava flows, CoAxial Segment, Juan de Fuca Ridge: evidence for multiple eruptions between 1981–1993. Geophysical Research Letters 22, 167–170.
Chadwick, W.W., Scheirer, D.S., Embley, R.W., Johnson, H.P., 2001. High-resolution bathymetric surveys using scanning sonars: lava flow morphology, hydrothermal vents, and geologic structure at recent eruption sites on the Juan de Fuca Ridge. Journal of Geophysical Research 106, 16075–16099.
Chiotis, E.D., Tsoutrelis, C.E., 1992. Estimation of the potential type of faulting in relation to the stress field: the North Aegean case study. Journal of Structural Geology 14, 215–223.
Cladouhos, T.T., Marrett, R., 1996. Are fault growth and linkage models consistent with power-law distributions of fault lengths? Journal of Structural Geology 18, 281–293.
Clifton, A.E., Schlische, R.W., 2001. Nucleation, growth, and linkage of faults in oblique rift zones: results from experimental clay models and implications for maximum fault size. Geology 29, 455–458.
Clifton, A.E., Schlische, R.W., 2003. Fracture populations on the Reykjanes Peninsula, Iceland: comparison with experimental models of oblique rifting. Journal of Geophysical Research 108 doi:2074, 10.1029/2001JB000635.
Clifton, A.E., Schlische, R.W., Withjack, M.O., Ackermann, R.V., 2000. Influence of rift obliquity in fault-population systematics: results of experimental clay models. Journal of Structural Geology 22, 1491–1509.
Corti, G., Bonini, M.I.F., Manetti, P., Mulugeta, G., 2001. Centrifuge models simulating magma emplacement during oblique rifting. Journal of Geodynamics 31, 557–576.
Cowie, P.A., Malinverno, A., Ryan, W.B.F., Edwards, M.H., 1994. Quantitative fault studies on the East Pacific Rise: a comparison of sonar imaging techniques. Journal of Geophysical Research 99, 15205–15218.
Crane, K., Doss, H., Vogt, P.R., Sundvor, E., Cherkashov, G., Poroshina, I., Joseph, D., 2001. The role of the Spitsbergen shear zone in determining morphology, segmentation and evolution of the Knipovich Ridge. Marine Geophysical Research 22, 153–205.
Crane, K., Solheim, A., 1995. Seafloor Atlas of the Northern Norwegian-Greenland Sea, vol. 137. Norsk Polarinstitutt, Oslo, Norway. 172.
Crane, K., Sundvor, E., Buck, R., Martinez, F., 1991. Rifting in the Northern Norwegian-Greenland Sea: thermal tests of asymmetric spreading. Journal of Geophysical Research 96, 14529–14550.
Curewitz, D., Karson, J.A., 1998. Geological consequences of dike intrusion at mid-ocean ridge spreading centers. In: Buck, W.R., Delaney, P.T., Karson, J.A., Lagabrielle, Y. (Eds.), Faulting and Magmatism at Mid-Ocean Ridges, vol. 106. American Geophysical Union, Washington D.C., pp. 117–136.
Dauteuil, O., Brun, J.-P., 1993. Oblique rifting in a slow-spreading ridge. Nature 361, 145–148.
Dauteuil, O., Brun, J.-P., 1996. Deformation partitioning in a slow spreading ridge undergoing oblique extension: Mohns Ridge, Norwegian Sea. Tectonics 15, 870–884.
Dauteuil, O., Huchon, P., Quemeneur, F., Souriot, T., 2001. Propagation of an oblique spreading centre: the western Gulf of Aden. Tectonophysics 332, 423–442.
Dawers, N.H., Anders, M.H., 1995. Displacement-length scaling and fault linkage. Journal of Structural Geology 17, 607–614.
DeMets, C., Gordon, R.G., Argus, D.F., Stein, S., 1990. Current plate motions. Geophysical Journal International 101, 425–478.
DeMets, C., Gordon, R.G., Argus, D.F., Stein, S., 1994. Effect of recent revisions to the geomagnetic time scale on estimates of current plate motion. Geophysical Research Letters 21, 2191–2194.
Dick, H., Lin, J., Schouten, H., 2003. An ultraslow-spreading class of ocean ridge. Nature 426, 405–412.
Dupin, J.-M., Sassi, W., Angelier, J., 1993. Homogeneous stress hypothesis and actual fault slip: a distinct element analysis. Journal of Structural Geology 15, 1033–1043.
Ebinger, C.J., Keir, D., Ayele, A., Calais, E., Wright, T.J., Belachew, M., Hammond, J.O.S., Campbell, E., Buck, W.R., 2008. Capturing magma intrusion and faulting processes during continental rupture: seismicity of the Dabbahu (Afar) rift. Geophysical Journal International. doi:10.1111/j.1365-246X.2008.03877.x.
Géli, L., Renard, V., Rommevaux, C., 1994. Ocean crust formation at very slow spreading centers: a model for the Mohns Ridge, near 72°N, based on magnetic, gravity, and seismic data. Journal of Geophysical Research 99, 2995–3013.
Gràcia, E., Charlou, J.L., Radford-Knoery, J., Parson, L.M., 2000. Non-transform offsets along the Mid-Atlantic Ridge south of the Azores (38°N–34°N): ultramafic exposures and hosting of hydrothermal vents. Earth and Planetary Science Letters 177, 89–103.
Gusev, E.A., Shkarubo, S.I., 2001. The anomalous structure of Knipovich Ridge. Russian Journal of Earth Science 3, 145–161.
Head, J.W., Wilson, L., Smith, D.K., 1996. Mid-ocean ridge eruptive vent morphology and structure: evidence for dike widths, eruption rates, and evolution of eruptions and axial ridges. Journal of Geophysical Research 101, 28265–28280.
Klingelhöfer, F., Géli, L., White, R.S., 2000. Geophysical and geochemical constraints on crustal accretion at the very-slow spreading Mohns Ridge. Geophysical Research Letters 27, 1547–1550.
Kuo, B.Y., Forsyth, D.W., 1988. Gravity anomalies of the ridge-transform system in the South Atlantic between 31° and 34,5°S: upwelling centers and variations in crustal thickness. Marine Geophysical Research 10, 205–232.
Lin, J., Purdy, G.M., Schouten, H., Sempéré, J.-C., Zervas, C., 1990. Evidence from gravity data for focused magmatic accretion along the Mid-Atlantic Ridge. Nature 344, 627–632.
Macdonald, K.C., 1982. Mid-ocean ridges: fine-scale tectonic, volcanic and hydrothermal processes within the plate boundary zone. Annual Reviews of the Earth and Planetary Sciences 10, 155–190.
Macdonald, K.C., Fox, P.J., Perram, L.J., Esien, M.F., Haymon, R.M., Miller, S.P., Carbotte, S.M., Cormier, M.H., Shor, A.H., 1988. A new view of the mid-ocean ridge from the behavior of ridge-axis discontinuities. Nature 335, 217–225.
Macdonald, K.C., Scheirer, D.S., Carbotte, S.M., 1991. Mid-Ocean Ridges: discontinuities, segments and giant cracks. Science 253, 986–994.
Mart, Y., Dauteuil, O., 2000. Analogue experiments of propagation of oblique rifts. Tectonophysics 316, 121–132.
McAllister, E., Cann, J., Spencer, S., 1995. The evolution of crustal deformation in an oceanic extensional environment. Journal of Structural Geology 17, 183–199.
Murton, B.J., Parson, L.M., 1993. Segmentation, volcanism and deformation of oblique spreading centres: a quantitative study of the Reykjanes Ridge. Tectonophysics 222, 237–257.

Okino, K., Curewitz, D., Asada, M., Tamaki, K., Vogt, P., Crane, K., 2002. Preliminary analysis of the Knipovich Ridge segmentation: influence of focused magmatism and ridge obliquity on an ultraslow spreading system. Earth and Planetary Science Letters 202, 275–287.

Olesen, O.G., Gellein, J., Habrekke, H., Kihle, O., Skilbrei, J.R., Smethrust, M.A., 1997. Magnetic anomaly map, Norway and adjacent ocean areas. Geological Survey of Norway.

Parson, L., Gràcia, E., Coller, D., German, C., Needham, D., 2000. Second-order segmentation; the relationship between volcanism and tectonism at the MAR, 38°N-35°40′N. Earth and Planetary Science Letters 178, 231–251.

Peacock, D.C.P., Sanderson, D.J., 1991. Displacements, segment linkage and relay ramps in normal fault zones. Journal of Structural Geology 13, 721–733.

Reches, Z., 1983. Faulting of rocks in three-dimensional strain fields II. Theoretical analysis. Tectonophysics 95, 133–156.

Reches, Z., Dieterich, J.H., 1983. Faulting of rocks in three-dimensional strain fields I. Failure of rocks in polyaxial, servo-control experiments. Tectonophysics 95, 111–132.

Rubin, A.M., 1992. Dike-induced faulting and graben subsidence in volcanic rift zones. Journal of Geophysical Research 97, 1839–1858.

Rubin, A.M., 1995. Propagation of magma-filled cracks. Annual Reviews of the Earth and Planetary Sciences 23, 287–336.

Rubin, A.M., Pollard, D.D., 1988. Dike-induced faulting in rift zones of Iceland and Afar. Geology 16, 413–417.

Sauter, D., Parson, L., Mendel, V., Rommevaux-Jestin, C., Gomez, O., Briais, A., Mével, C., Tamaki, K., The FUJI Scientific Team, 2002. TOBI sidescan sonar imagery of the very slow-spreading Southwest Indian Ridge: evidence for along-axis magma distribution. Earth and Planetary Science Letters 199, 81–95.

Searle, R.C., Cowie, P.A., Mitchell, N.C., Allerton, S., MacLeaod, C.J., Escartin, J., Russell, S.M., Slootweg, P.A., Tanaka, T., 1998a. Fault structure and detailed evolution of a slow spreading ridge segment: the Mid-Atlantic Ridge at 29°N. Earth and Planetary Science Letters 154, 167–183.

Searle, R.C., Keeton, J.A., Owens, R.B., White, R.S., Mecklenburgh, R., Parsons, B., Lee, S.M., 1998b. The Reykjanes Ridge: structure and tectonics of a hot-spot-influenced, slow-spreading ridge, from multibeam bathymetry, gravity and magnetic investigations. Earth and Planetary Science Letters 160, 463–478.

Sella, G.F., Dixon, T.H., Mao, A., 2002. REVEL: a model for recent plate velocities from space geodesy. Journal of Geophysical Research 107. doi:10.1029/2000JB000033.

Skogseid, J., Planke, S., Faleide, J.I., Pedersen, T., Eldholm, O., Neverdal, F., 2000. NE Atlantic continental rifting and volcanic margin formation. In: Nøttvedt, A. (Ed.), Dynamics of the Norwegian Margin. The Geological Society, London, vol. 167, pp. 285–326.

Schlische, R.W., Withjack, M.O., Eisenstadt, G., 2002. An experimental study of the secondary deformation produced by oblique-slip normal faulting. American Association of Petroleum Geologist Bulletin 86, 885–906.

Standish, J.J., Dick, H.J.B., Michael, P.J., Melson, W.G., O'Hearn, T., 2008. MORB generation beneath the ultraslow spreading Southwest Indian Ridge (9–25°E): major element chemistry and the importance of process versus source. Geochemistry Geophysics Geosystems 9, Q05004. doi:10.1029/2008GC001959.

Sundvor, E., Eldholm, O., Gladczenko, T.P., Planke, S., 2000. Norwegian-Greenland Sea thermal field. In: Nøttvedt, A. (Ed.), Dynamics of the Norwegian Margin. The Geological Society, London, vol. 167, pp. 397–410.

Tavarnelli, E., Pasqui, V., 2000. Fault growth by segment linkage in seismically acitve settings: examples from the Southern Apennines, Italy, and the Coast Ranges, California. Journal of Geodynamics 29, 501–506.

Taylor, B., Crook, K., Sinton, J., 1994. Extensional transform zones and oblique spreading centers. Journal of Geophysical Research 99, 19707–19718.

Tuckwell, G.W., Bull, J.M., Sanderson, D.J., 1996. Models of fracture orientation at oblique spreading centres. Journal of the Geological Society 153, 185–189. doi:10.1144/gsjgs.153.2.0185.

Vermilye, J.M., Scholz, C.H., 1999. Fault propagation and segmentation: insight from the microstructural examination of a small fault. Journal of Structural Geology 21, 1623–1636.

Vogt, P.R., Jung, W.-Y., Brozena, J., 1998. Arctic margin gravity highs: deeper meaning for sediment depocenters? Marine Geophysical Research 20, 459–477.

Vogt, P.R., Sundvor, E., 1996. Heat flow highs on the Norwegian-Barents-Svalbard continental slope: deep crystal fractures, dewatering, or "memory in the mud"? Geophysical Research Letters 23, 3571–3574.

Withjack, M.O., Jamison, W.R., 1986. Deformation produced by oblique rifting. Tectonophysics 126, 99–124.

Wright, D.J., 1998. Formation and development of fissures at the East Pacific Rise: implications for faulting and magmatism at mid-ocean ridges. In: Buck, W.R., Delaney, P.T., Karson, J.A., Lagabrielle, Y. (Eds.), Faulting and Magmatism at Mid-Ocean Ridges, vol. 106. American Geophysical Union, Washington D.C., pp. 137–151.

Wright, D.J., Haymon, R.M., Macdonald, K.C., 1995. Breaking new ground: estimates of crack depth along the axial zone of the East Pacific Rise (9°12′–54′N). Earth and Planetary Science Letters 134, 441–457.

Wright, D.J., Haymon, R.M., White, S.M., Macdonald, K.C., 2002. Crustal fissuring on the crest of the Southern East Pacific Rise, 17°15′–40′S. Journal of Geophysical Research 107. doi:10.1029/2001JB000544.